A Geomechanics Approach to Evaluate Gas Shale Frackability: A Case Study with the Woodford Shale*

Minh H. Tran[1], Shengli Chen[1], Sierra P. Rafael[2], Younane N. Abousleiman[1,2], and Roger M. Slatt[2]

Search and Discovery Article #50913 (2014)
Posted January 27, 2014

*Adapted from extended abstract prepared in conjunction with poster presentation at AAPG Annual Convention and Exhibition, Long Beach, California, April 22-25, 2012, AAPG©2012

[1]Mewbourne School of Petroleum and Geological Engineering, University of Oklahoma, Norman, OK (tranhaminh83@ou.edu)
[2]ConoPhillips School of Geology and Geophysics, University of Oklahoma, Norman, OK

Abstract

In addition to the TOC, the brittleness of the shale formation has recently been used as a deciding factor for identifying prospect intervals for fracturing stimulation. This paper provides a geomechanics approach to quantify gas shale frackability taking into account the transversely isotropic nature of shales. In addition, geomechanics explanations are given for the field observations that hydraulic fracturing in clay-rich and finely laminated intervals produce less microseism than in quartz-rich and coarsely laminated intervals.

In this study, the shales frackability is evaluated based on groups of anisotropic elastic moduli that control the fracture gradient and fracture length growth in shale formations. The approach is illustrated with the results from geomechanics and geological characterizations of the Oklahoma Woodford shale. In particular, the preserved Woodford samples were prepared for laboratory characterizations including thin sections, XRD, UPV, UCS, tensile strength, and fracture toughness with microseism recorded during testing. The anisotropic geomechanics properties were modeled with correlations to mineralogy from XRD and well logs, then, ultimately used to estimate the fracture gradient and fracture length profiles.

Inverse proportional relations of elastic stiffnesses with clay and organic content were clearly observed with lab measurements and captured in the upscaling model. The results also showed that lower Poisson's ratio and higher Young's modulus gives lower fracture gradient and longer fracture length indicating a more brittle formation. Moreover, incorporate the shales anisotropic properties into modeling was shown to significantly increase the ability to resolve the brittle-ductile couplets at parasequence scale. Finally, finite element analyses for stresses distributions near the fracture opening in anisotropic and layered formations implied that the observed high microseism in quartz-rich and coarsely laminated intervals is the result of a combination of interlayer shearing and higher fracture shear stress concentration for the lower anisotropy shale.

The outcomes of this study finally explain the field observations that high quartz content or a combination of high Young's modulus and low Poisson's ratio may indicate a brittle formation. They also constitute a geomechanics consistent framework for quantitative evaluation of gas shale frackability at the parasequence scale taking into account the shales intrinsic anisotropy.

Introduction

In addition to the TOC, the brittleness of the shale formation has recently been used as a deciding factor for identifying prospect intervals for fracturing stimulation. Existing studies have attempted to correlate the brittleness of the shale formations to the elastic moduli or clay content which will allow the identification of brittle and ductile intervals based on gamma ray (GR) logs, sonic logs and seismic interpretation (Rickman et al., 2008; Harris et al., 2011; Slatt and Abousleiman, 2011). It is noteworthy that the term "brittleness" used in these studies refers to the ease to induce a hydraulic fracture in the formation, also known as formation frackability, rather than the conventional mechanics definition for brittle and ductile materials. For example, based on field observations in the Barnett Shale, Rickman et al. (2008) have correlated that a combination of high Young's modulus and low Poisson's ratio indicates a brittle formation. It should also be noticed that the well-known anisotropic nature of shales has not been incorporating in these correlations.

In this work, a geomechanics approach to quantify gas shale brittleness taking into account the transversely isotropic nature of shales is proposed. The approach is then applied to evaluate the frackability of the Woodford shale using well logs and laboratory data obtained from a shallow behind quarry well drilled in near the Arkoma basin, Oklahoma. The results show that lower Poisson's ratio and higher Young's modulus gives lower fracture gradient and longer fracture length, hence, indicating a more brittle formation. In addition, it is observed that higher clay or kerogen content can result in a shorter fracture length. This is a consequence of the inverse proportional relation between elastic moduli and clay/kerogen content. This observation hints the possibility to use GR log as preliminary assessment method to identify brittle and ductile couplets as shown in Slatt and Abousleiman (2011). Last but not least, the analyses show that incorporate the shales anisotropic properties into modeling can significantly increase the ability to resolve the brittle-ductile couplets at parasequence scale.

Finally, field observations and our laboratory tests show that quartz-rich and coarsely laminated intervals generally produce high level of acoustic emissions during fracturing. Finite element modeling (FEM) is conducted to explain the observation. The results show that the observed high level of acoustic emissions may result from a combination of interlayer shearing and higher fracture shear stress concentration for the low clay content shales.

The Effects of Anisotropic Elastic Moduli on Fracture Gradient

An existing fracture opens and propagates if the fracturing fluid creates at the fracture tip a tensile stress exceeding the sum of the effective minimum horizontal principal stress, denoted as $S_h^{'}$, and the formation tensile strength, denoted as T_o. The sum of $S_h^{'}$ and T_o normalized to the formation depth shall be referred to as the fracture gradient (FG)

$$FG = \frac{S_h^{'} + T_o}{D} = \frac{S_h - \alpha_1 P + T_o}{D} \tag{1}$$

where S_h is the total minimum horizontal principal stress, P is the formation pore pressure, α is the Biot's pore pressure coefficient in direction parallel to formation bedding planes, and D is the formation depth. As most gas formations are at depths greater than a few thousands feet, $S_h^{'}$ is usually much larger than T_o and becomes a dominant factor for FG determination. For a transversely isotropic shale formation with horizontal laminations subjected to overburden stress and in a region with negligible tectonic activities, $S_h^{'}$ can be estimated as follows

$$S_h^{'} = \frac{E_1}{E_3}\frac{\nu_3}{1-\nu_1}\left(S_v - \alpha_3 P\right) \tag{2}$$

with E, ν, and α are respectively the Young's modulus, Poisson's ratio, and Biot's pore pressure coefficient. The subscript "1" and "3" denote properties in direction parallel and perpendicular to the bedding planes. It is obvious from Eq. 2 that smaller values of ν_1 and ν_3 gives smaller $S_h^{'}$ and, hence, lower the fracture gradient. Although the uniaxial strain model is not applicable in tectonically active basins and calibrations with other methods should be conducted, the simple form of Eq. 2 makes it an appealing method for preliminary assessment of the formation fracture gradient using well logs.

The Effects of Formation Anisotropy on Fracture Length

Shown in Figure 1 is the geometry of a linear vertical fracture in a horizontally laminated shale formation following the GdK (Geerstma and de-Klerk, 1969) and the PKN (Perkins and Kern, 1961; Nordgren, 1972) model.

Since the GdK model assumes a state of plane strain in the direction parallel to the formation bedding planes, the maximum fracture width at the wellbore, w_o^{GdK}, naturally becomes $w_o^{GdK} = 2(1-\nu_1^2)L\Delta p / E_1$ according to Sneddon (1946). Δp is the difference between the hydraulic fracturing fluid pressure and minimum horizontal stress. E_1 and ν_1 are the elastic moduli in direction parallel to the bedding planes. Assuming that the fracturing fluid leak-off is negligible due to the intrinsically low permeability of shale formations, the GdK fracture length is given as

$$L^{GdK} = 0.68\left(\frac{E_1 Q^3}{\mu(1-\nu_1^2)h_f^3}\right)^{1/6} t^{2/3} \tag{3}$$

where Q is the injection rate, μ is the viscosity of the fracturing fluid, h_f is the fracture height, and t is the pumping time.

For the PKN model, w_o^{PKN} can be a function of E_1, E_3, G_3, ν_1, ν_3. In this work, finite element method modeling with ABAQUS is used to analyze the sensitivity of the anisotropic elastic moduli on w_o^{PKN} as shown in Figure 2. The analysis revealed that among the five independent anisotropic elastic parameters, E_1 is the most dominant factor and the fracture width is approximately inversely proportional to the anisotropic

ratio of E_1/E_3. Hence, as a first order approximation, the expression for w_o^{PKN} is $w_o^{PKN} = (1-\nu_1^2)h_f \Delta P / E_1$. Consequently, the PKN fracture length with negligible fracturing fluid leak-off is as follows

$$L^{PKN} = 0.68\left(\frac{E_1 Q^3}{\mu(1-\nu_1^2)h_f^4}\right)^{1/5} t^{4/5} \tag{4}$$

Since ν_1 enters the expression for fracture length as $1-\nu_1^2$ and the Poisson's ratios of rocks are typically between 0.1 and 0.35, the effects of ν_1 on L are insignificant. Hence, the higher the formation Young's modulus, the longer the fracture length for a given pumping rate and time.

Geomechanics Evaluation of Gas Shale Frackability using Well-Logs

The above analysis explains why the field observations that a combination of high Young's modulus and low Poisson's ratio may give indications for brittle intervals. In addition, the analysis shows that estimation of gas shale formations frackability requires not only the elastic and poroelastic properties in direction perpendicular to bedding planes but also those in direction parallel to bedding planes. Although sonic logs are routinely employed to estimate the mechanical properties of subsurface formations, unfortunately, even the most advanced sonic log cannot obtain the full set of formation anisotropic elastic and poroelastic properties. Due to their vertical setup, sonic logs cannot be used to obtain the mechanical properties in any direction that is not parallel to the borehole axis. This inability of sonic logs to capture the full set of shale formation transversely isotropic elastic moduli may lead to inaccurate determination of fracture gradient and fracture length. For example, since sonic logs run in a vertical wellbore can only report E_3, an underestimation of fracture length will occur as $E_3 < E_1$. Indeed, it has been reported that simulated hydraulic fracture length is often shorter than the true fracture length as hydraulic fractures from the treated wellbores frequently intersect with adjacent boreholes.

Advances in nano-technology when applied to study shale mechanical properties have allowed measurements of shale mechanical properties at a scale that have never been observed (100 nm-100 μm) and have revealed so much about the mechanical interaction of shale constituents at the nano-scale. Figure 3 shows the schematic of a nano-indenter, the force-displacement curve from a nano-indentation test, and an Atomic Force Microscope (AFM) image of a nano-indention with dimensions of 4 μm × 4 μm on the surface of a Woodford sample.

Figure 4 displays the plot of the indentation moduli when indented parallel, M_1, and perpendicular, M_3, to samples bedding planes versus the clay packing density, η, obtained from over 5400 nano-indentation tests on seven different shale species excluding the Woodford shale. Figure 4 has evidently shown that the clay representative elementary volume (REV) is anisotropic as the extrapolated M_1 and M_3 to $\eta = 1$ are different. It can also be observed that both M_1 and M_3 reduce to 0 (no apparent force transmission in the material) at approximately 0.5 clay packing density, which suggests that the clay REV can be represented as spheres within the framework of micromechanics modeling (Ulm and Abousleiman, 2006). Based on the aforementioned experimental observations, an upscaling model, so called the GeoGenome model, has been constructed for an anisotropic nano-granular material based on a micro-poromechanics approach (Ortega et al., 2007; Ortega et al., 2009). In

this model, the macroscopic elastic and poroelastic properties of shale rocks are a function of the clay packing density, η, the volume fraction of the non-clay phase, f_{inc}, and the organic volume fraction, f_{org}. These inputs can be calculated directly from formation porosity and mineralogy composition, which are readily reported by advanced geochemical logs such as the GEM Elemental Analysis Tool of Halliburton, the Element Capture Spectroscopy (ECS) of Schlumberger, etc as follows

$$f_{inc} = \frac{(1-\phi)\sum_{k=1}^{total\ non-clay} \frac{m_k}{\rho_k}}{\sum_{k=1}^{total\ non-clay} \frac{m_k}{\rho_k} + \sum_{l=1}^{total\ clay} \frac{m_l}{\rho_l}}, \eta = 1 - \frac{\phi}{1-f_{inc}}, \quad f_{org} = \frac{\sum_{n=1}^{total\ organic} \frac{m_n}{\rho_n}}{\sum_{l=1}^{total\ clay} \frac{m_l}{\rho_l} + \sum_{n=1}^{total\ organic} \frac{m_n}{\rho_n}} \tag{5}$$

where m, ρ, ϕ are the mass percent, density, and porosity respectively. The subscripts "k", "l", and "n" indicate the non-clay phase, the clay phase, and the organic phase respectively.

The GeoGenome model and the above analysis form a protocol for log-based evaluations of gas shale frackability, which can be summarized as follows:

- Estimate and calibrate the formation anisotropic elastic and poroelastic properties with data from geochemical logs and sonic logs.
- Evaluate the fracture gradient profile along the well.
- Evaluate fracture length profile by plotting the group $E_1/(1-v_1^2)$.
- Intervals with low fracture gradient and sandwiched between two layers of higher fracture gradients will promote the fracture length growth as the fracture height growth is contained (fracture containment).
- For those intervals, ones with larger $E_1/(1-v_1^2)$ will yield longer fracture length.

Applications to Woodford Shale Characterization

In this work, a shallow well (70 m) in a Woodford quarry, Oklahoma, USA was cored and logged. The formation mineralogy compositions and porosity reported by the ECS log and the porosity logs were used as inputs in the GeoGenome model to obtain the Woodford formation anisotropic elastic and poroelastic properties. The Sonic Scanner log responses and Ultrasonic Pulse Velocity (UPV) measurements on core samples were used to validate the simulated results. In addition, Woodford Shale fracturing properties were obtained through a suite of Brazilian Tensile and Chevron Notched Semicircular Bend (CNSCB) tests on the preserved core samples. Last but not least, the acoustic emission (AE) was also recorded during the CNSCB tests to facilitate study about microseism in gas shale. Details on the experiments and calibrations of well-logs data can be found in Abousleiman et al. (2007, 2009), and Sierra et al. (2010).

Upscaling for Woodford shale anisotropic elastic properties from geochemical log

Figure 5 shows Woodford formation mineralogy compositions as reported by the ECS log. Also shown in Figure 5 are the reported porosity from well log, ϕ_{log}, together with the Hg-injection porosities, ϕ_{Hg}, and the adjusted log porosity, $\phi_{log\ adjusted}$, after calibrated with Hg-injection porosities.

Displayed in Figure 6 and Figure 7 are the simulated anisotropic elastic and poroelastic properties compared to the Sonic Scanner log responses and the laboratory UPV measurements. The dashed lines in each plot are the simulated variations of the results assuming 10% uncertainties in mineralogy composition and porosity. The qualitative and quantitative agreement between the simulated results and UPV measurement as well as Sonic Scanner log have demonstrated the applicability of the GeoGenome model for estimating gas shale formation anisotropic elastic and poroelastic properties. It should be noticed from Figure 7 that E_1 and α_1, which required a complete characterization of a transversely isotropic formation, were not given by the Sonic Scanner as the setup of the sonic sonde only allows the extraction of properties in direction parallel to the borehole axis.

Woodford shale anisotropic tensile strength and fracture toughness

The Woodford shale anisotropic tensile strength was determined with the Brazilian tensile tests. Figure 8 shows the schematic of the experiment setup, the picture of a Woodford sample under Brazilian test, and two tested samples after loading perpendicular and parallel to the bedding planes.

Figure 9 is a summary of the Brazilian test results on Woodford shale samples and the simulated Woodford shale anisotropic tensile strength. The tensile strength correlations assume that tensile strength is 10% of the unconfined compressive strength (UCS) and the relation between UCS and E_3 follows Chang et al. (2004). Detail derivation can be found in Sierra (2011).

Figure 10 is the schematic of the experimental set up and a prepared Woodford sample for the CNSCB fracture toughness test. The fracture toughness is a quantity describing the resistance of the material to the propagation of a preexisting crack. In this experiment, the preexisting crack (notch) was cut at 90° with respect to the base of the specimen and forms a plane orthogonal to the sample bedding planes. This configuration of the preexisting crack simulates the opening of vertical hydraulic fractures from horizontal wellbores. As noted in Figure 10, two pairs of 600 kHz compressional piezoelectric crystals were mounted on each side of the sample and in front of the crack to monitor the acoustic emissions from the fracturing process. Table 1 summarizes the fracture toughness of samples from Upper, Middle, and Lower Woodford. The results show insignificant variation of fracture toughness between samples from the same interval. However, when comparing the lower clay Upper Woodford to the more clay rich Middle and Lower Woodford, there is an increase, up to 57%, in the fracture toughness.

Evaluation of Woodford shale frackability

The left log track in Figure 11 is the calculated S_h using the simulated anisotropic elastic/poroelastic properties and log reported formation density. The formation top is assumed to be at 1,830 m (6,000 ft) following what has been reported for common depth of Woodford shale in Arkoma basin. The pore pressure gradient is assumed to be 0.01 MPa/m (0.43 psi/ft). Calculation ignoring the formation anisotropy is also

included to illustrate the effects of anisotropic properties on the estimation of S_h (hence FG). Clearly, incorporating shales anisotropic properties into modeling can significantly increase the resolution of S_h profile and, hence, the FG profile. The two log tracks in the middle of Figure 11 are the calculated fracture gradient (FG) taking into account the formation anisotropy and the estimated fracture length profile reflected through the group $E_1/(1-v_1^2)$. Comparing the fracture length profile with the mineralogy log track shows that higher kerogen content leads to shorter fracture length. Since kerogen is a soft material, higher kerogen content results in a more compliance rock or lower $E_1/(1-v_1^2)$. Similar effects are also applicable for high clay content intervals as the clay REV is more compliance than the non-clay inclusions such as quartz, feldspar, etc. The inverse proportional relation between elastic moduli and kerogen, clay content has been successfully captured in the GeoGenome model.

Based on the simulated FG, the Middle Woodford and Lower Woodford intervals both promote hydraulic fracture to grow in length as they contain a region with low FG sandwiched between layers of higher FG. The fracture toughness test results also suggest that the growth of fractures in the Middle and Lower Woodford intervals are much easier than in the Upper Woodford interval. Based on the simulated fracture length profile, the fracture length in the Middle Woodford is consistently longer than those in the Lower Woodford. Hence, the analyses show that the Middle Woodford is most favorable for fracture development, followed by the Lower Woodford.

Micro-Seismism in Gas Shale Formation

Figure 12 shows the acoustic emissions (AE) recorded during CNSCB tests. The moment of the uncontrollable fracture growth is indicated by the maximum number of emissions per unit time in all diagrams. The results show that less acoustic emissions were recorded prior to sample failure for the more clay rich samples. In addition, comparing the acoustic emission results with thin sections from the tested samples showed that finely laminated samples also produce lower acoustic emissions prior to sample failure.

Warpinski (1994) suggested, “All evidence available suggests that microseisms are generated by shear movement of the rock in the vicinity of the hydraulic fracture”. Therefore, investigations for the mechanism of the aforementioned observation are, indeed, study for the effects of lamination and anisotropy (high clay content results in more anisotropic formation) on shear stress distribution at the vicinity of the fracture. Figure 13 shows a schematic of a fracture opening and the corresponding FEM model built in ABAQUS. Figure 14 is the plot of shear stress distribution near the fracture face for a single layer fracture zone at different anisotropy ratio of E_1/E_3 and G_1/G_3. The results show that the higher the anisotropy ratio, the lower the maximum shear stress (Tresca stress) at the fracture tip. Therefore, high clay content intervals produce less acoustic emissions during fracturing.

On the other hand, Figure 15 is the plot of shear stress distribution along a layers interface in a formation assumed to contain 3 layers and 9 layers with alternating isotropic elastic properties. Also shown in Figure 15 is the shear stress distribution along the same path for a homogenous transversely isotropic formation. This case corresponds to formation with very fine layers such that even each layer is isotropic, the whole formation exhibits transverse isotropy following Backus’s average (Backus, 1962). The results show that, for the same fracture height, a formation with finer lamination produces less shear stress along the interface of layers. Consequently, less acoustic emissions will be observed in finely laminated intervals during fracturing.

Conclusions

In this work, a geomechanics approach to evaluate gas shale frackability is proposed and applied to evaluate the Woodford shale formation using log and core data obtained from a well drilled in a quarry near Arkoma basin, Oklahoma. The analyses show that the Middle Woodford is most favorable for fracture development, followed by the Lower Woodford. It is observed that higher clay or kerogen content can result in shorter fracture length. This observation hints the possibility to use GR log as preliminary assessment method to identify brittle and ductile couplets. In addition, incorporating shales anisotropic properties into modeling can significantly increase the ability to resolve the brittle-ductile couplets at parasequence scale. Finally, finite element modeling (FEM) is conducted to explain the observations that hydraulic fracturing in quartz-rich and coarsely laminated intervals generally produces high level of acoustic emissions. The analysis indicates that this observation may be the result of interlayer shearing and higher fracture shear stress concentration for the lower clay content shale.

Acknowledgement

This work is partially funded by the Geomechanics Gas Shale Consortium at the University of Oklahoma.

Selected References

Abousleiman, Y., M. Tran, S. Hoang, C. Bobko, A. Ortega, and F-J. Ulm, 2007, Geomechanics field and laboratory characterization of the Woodford Shale: The Next Gas Play: SPE 110120.

Abousleiman, Y.N., M.H. Tran, S.U. Hoang, A. Ortega, and F-J. Ulm, 2009, Geomechanics field characterization of the two prolific US mid-west gas plays with advanced wire-line logging tools: Paper SPE 124428.

Backus, G.F., 1962, Long-wave elastic anisotropy produced by horizontal layering: Journal Geophysical Research, v. 67, p. 4427-4441.

Geerstma, J., and F. de-Klerk, 1969, A rapid method of predicting width and extent of hydraulically induced fractures: Journal of Petroleum Technology, December, p. 1571-1581.

Harris, N. B., J.L. Miskimins, and C.A. Mnich, 2011, Mechanical anisotropy in the Woodford Shale, Permian Basin: origin, magnitude, and scale: The Leading Edge, Mar. 2011, p. 284-291.

Rickman, R., M. Mullen, E. Petre, B. Grieser, and D. Kundert, 2008, A practical use of shale petrophysics for stimulation design optimization: SPE Paper #115258, 11 p.

Nordgren, R. P., 1972, Propagation of a vertical hydraulic fracture: SPEJ, August 1972, p. 306-314.

Ortega, A.J., F-J. Ulm, and Y.N. Abousleiman, 2007, The effect of the nanogranular nature of shale on their poroelastic behavior: Acta Geotechnica, v. 2, p. 155-182.

Ortega, A.J., F-J. Ulm, and Y.N. Abousleiman, 2009, The nanogranular acoustic signature of shale: Geophysics, v. 74, p D65-D84.

Perkins, T.K., and L.R. Kern, 1961, Widths of hydraulic fractures: Journal of Petroleum Technology, September, p. 937-949.

Ulm, F-J., and Y.N. Abousleiman, 2006, The Nanogranular Nature of Shale: Acta Geotechnica, v. 1, p. 77-88.

Sierra, R., M.H. Tran, Y.N. Abousleiman, and R.M. Slatt, 2010, Woodford Shale Mechanical Properties and the Impacts of Lithofacies: 44th US Rock Mechanics Symposium and 5th US-Canada Rock Mechanics Symposium, Salt Lake City, Utah, American Rock Mechanics Association, 10 p.

Sierra-Perez, R.P., 2011, Integrated geomechanics and geological characterization of the Devonian-Mississippian Woodford Shale: Master Thesis University of Oklahoma, 110 p.

Slatt, R.M. and Y. Abousleiman, 2011, Merging sequence stratigraphy and geomechanics for unconventional gas shales, *in* B. Hart, C.M. Sayers, and A. Jackson, eds., Shales: Leading Edge, v. 30/3, p. 274-282.

Sneddon, I.N., 1946, The distribution of stress in the neighborhood of a crack in an elastic solid: Proceedings of the Royal Society of London, v. 187, p. 229-260.

Warpinski, R. N. 1994. Interpretation of hydraulic fracturing mapping experiment: SPE 27985. Doi: 10.2118/27985-MS.

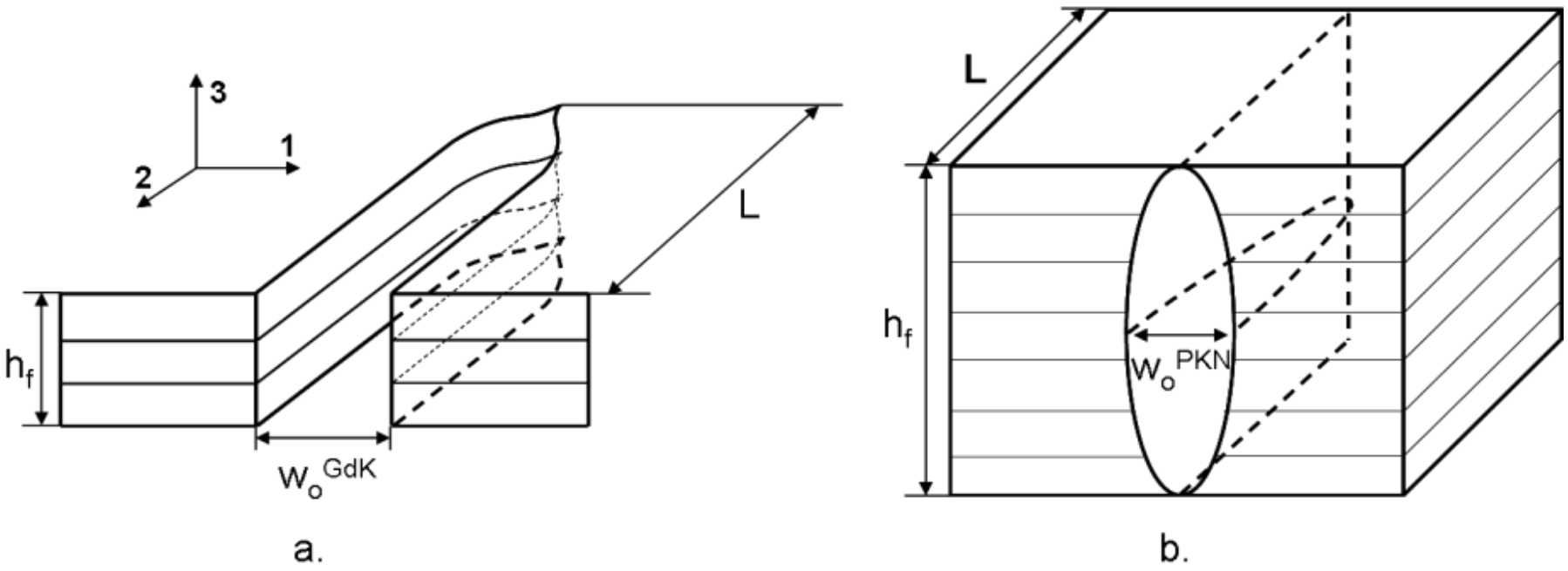

Figure 1. Schematic of a) GdK fracture, b) PKN fracture.

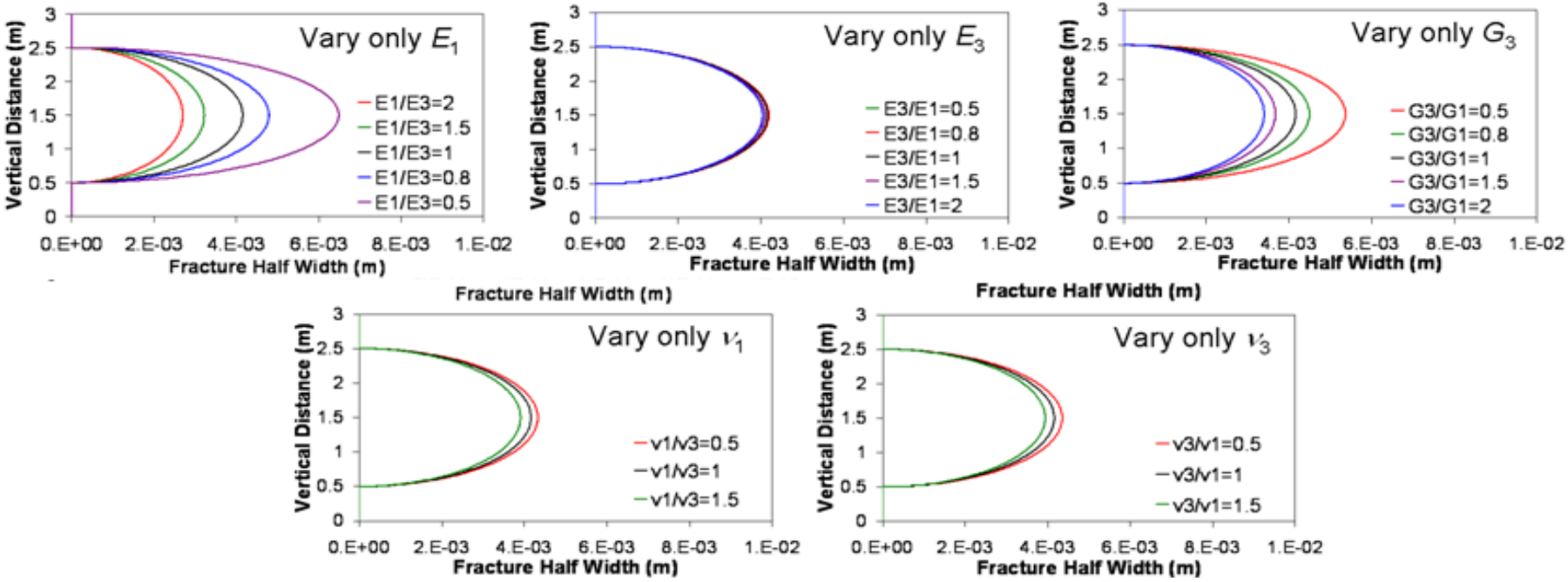

Figure 2. The sensitivity of anisotropic elastic properties on w_o^{PKN} .

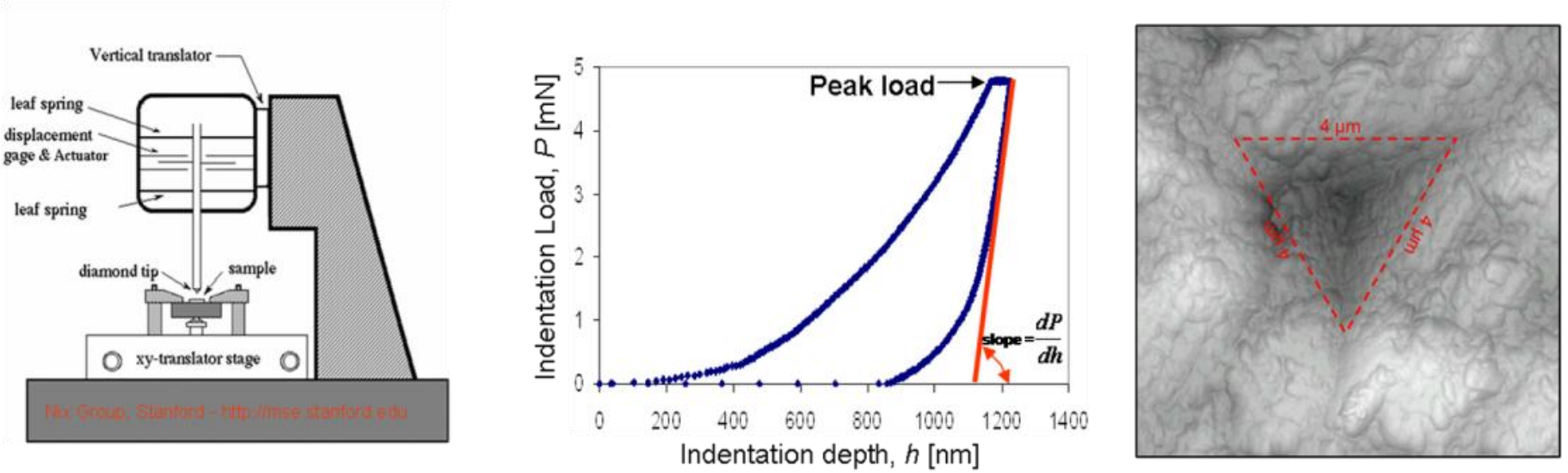

Figure 3. Schematic of nano-indenter, a load-displacement curve from nano-indentation test on Woodford shale sample, and AFM picture of indented cone on a Woodford sample.

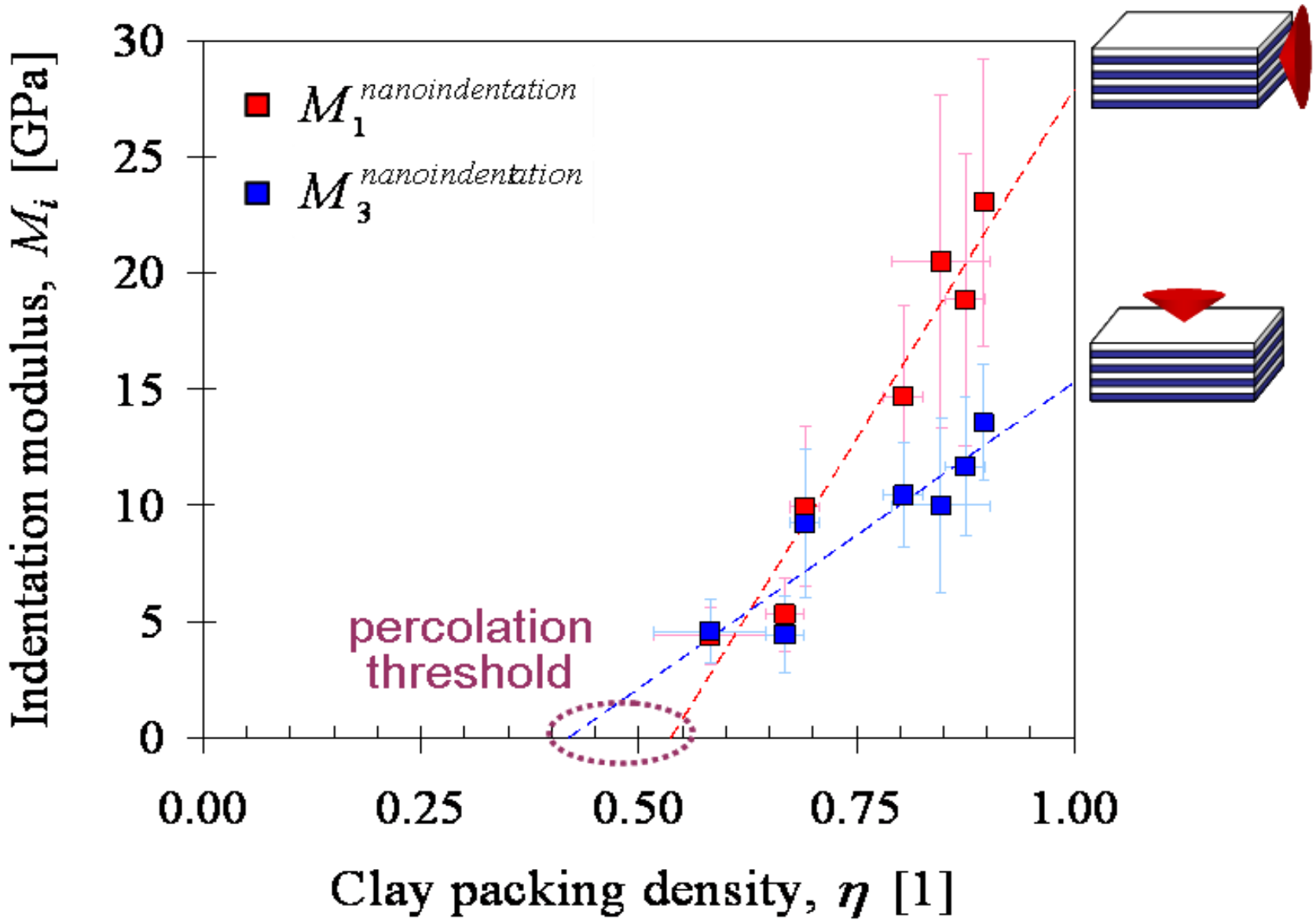

Figure 4. Indentation moduli versus clay packing density from nano-indentation tests on shale samples.

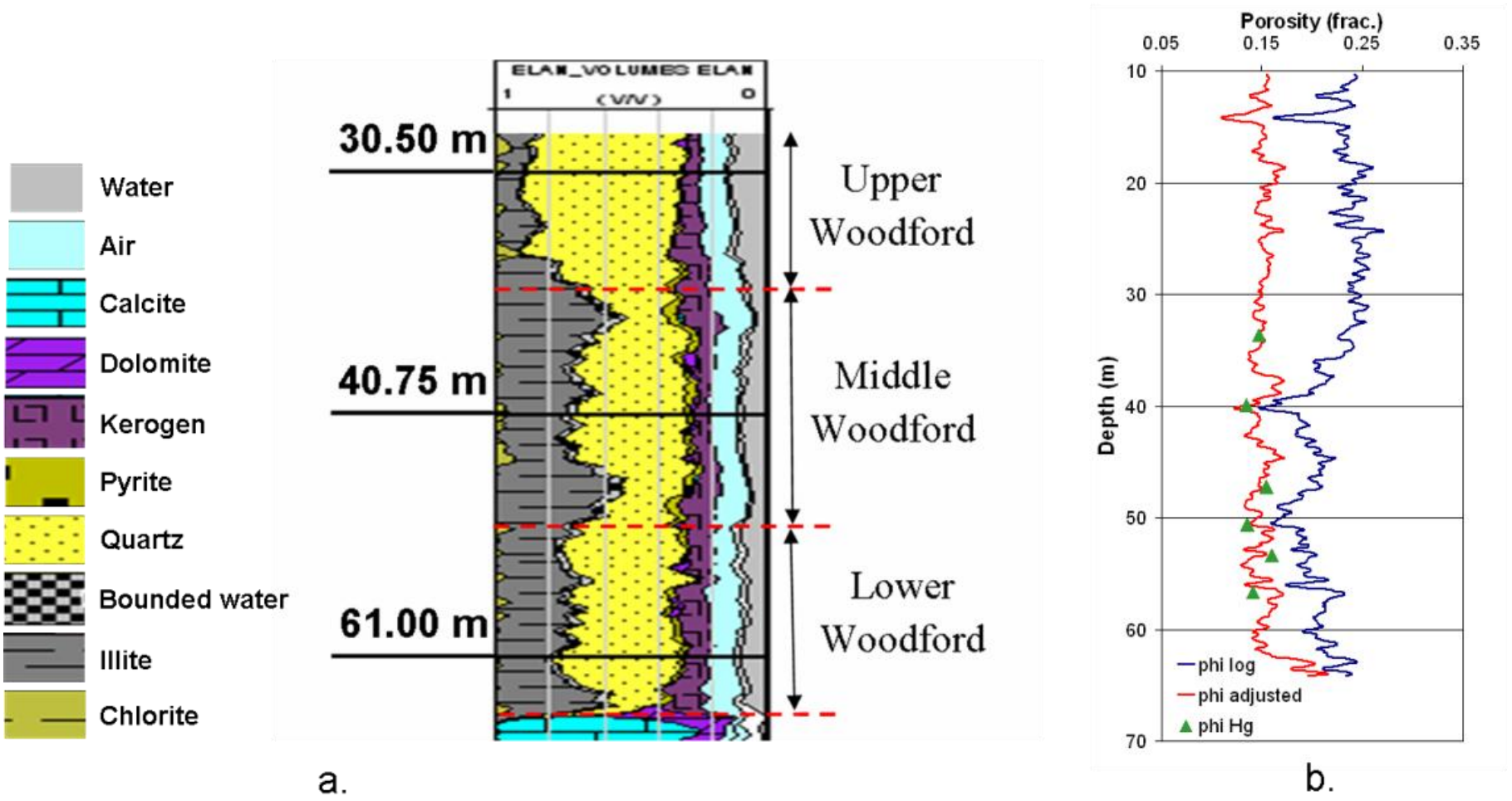

Figure 5. Mineralogy and porosities of the Woodford formation.

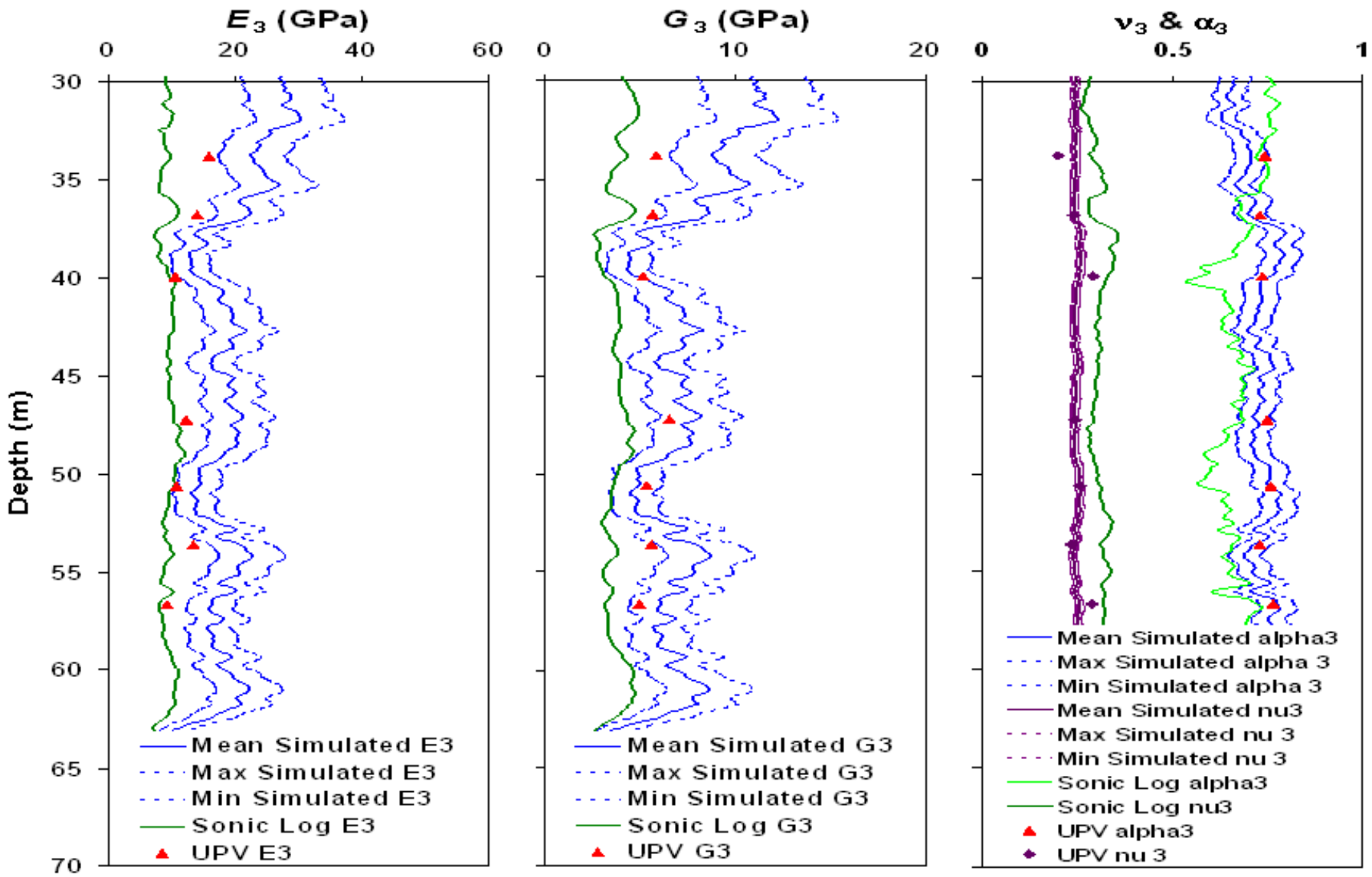

Figure 6. Simulated Woodford shale elastic and poroelastic properties in direction perpendicular to formation bedding planes.

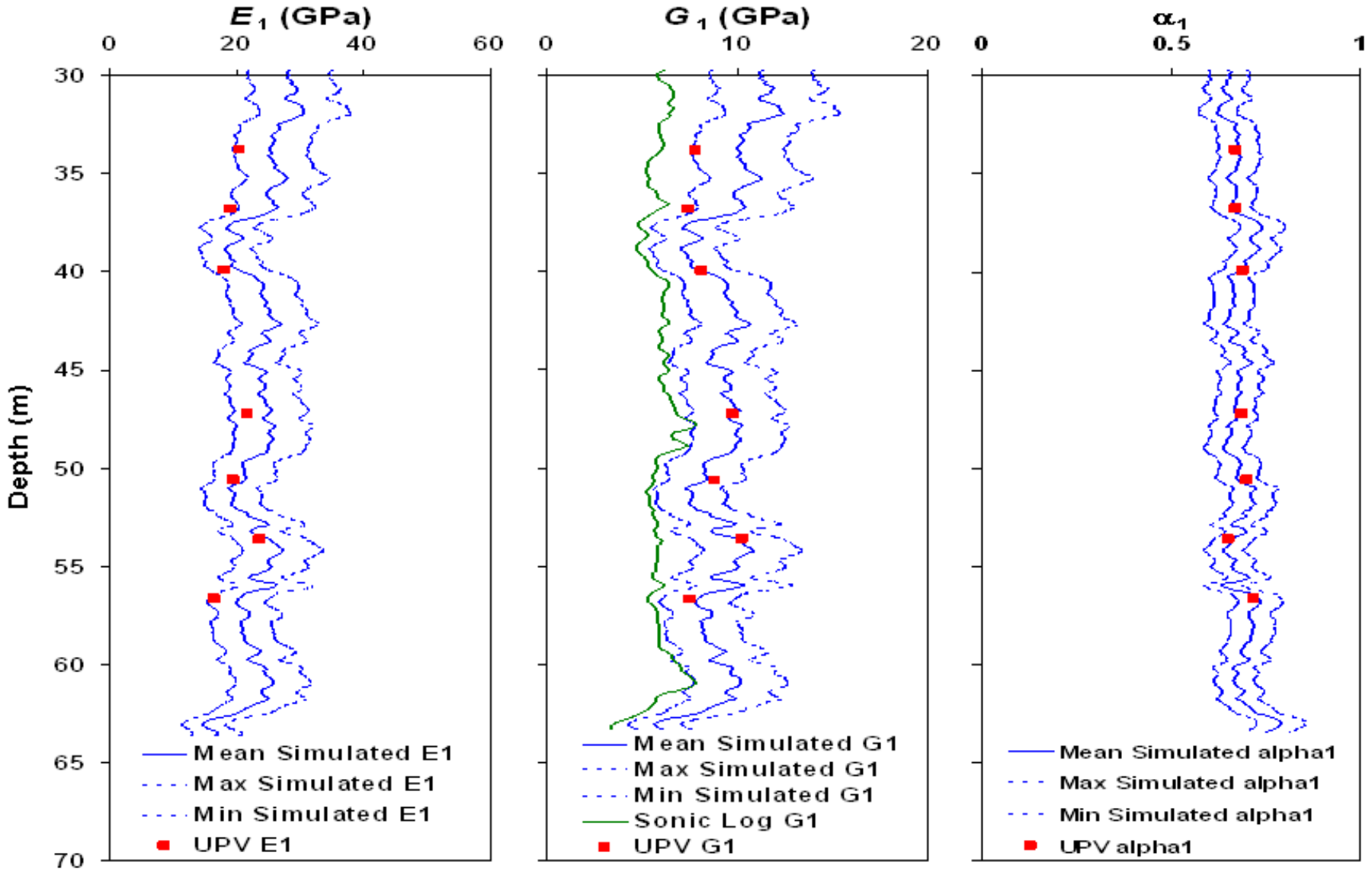

Figure 7. Simulated Woodford shale elastic and poroelastic properties in direction parallel to formation bedding planes.

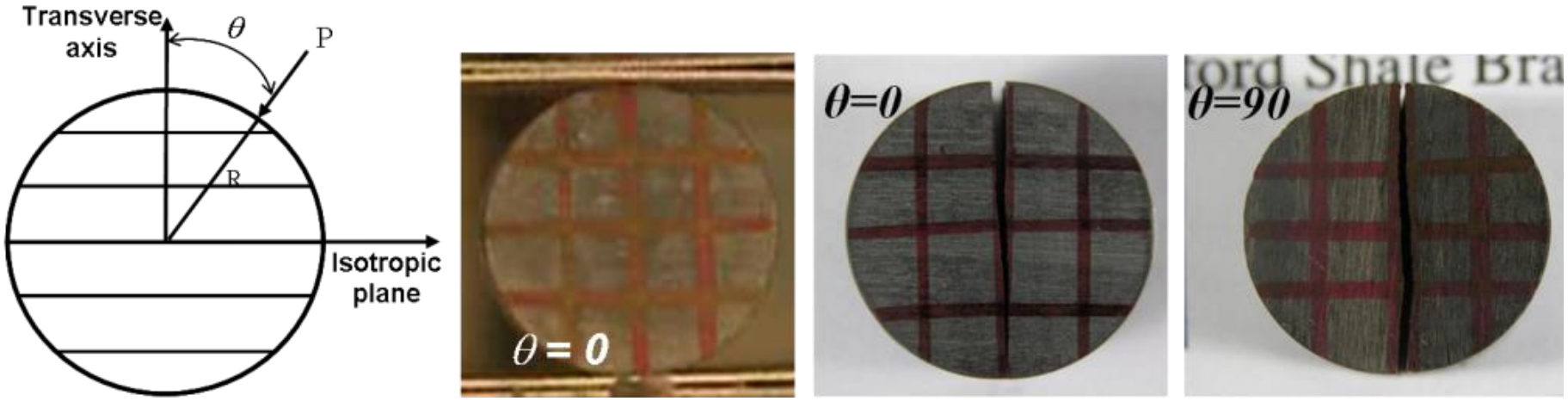

Figure 8. Schematic of the Brazilian tensile test set up, a Woodford sample during test, and tested Woodford samples.

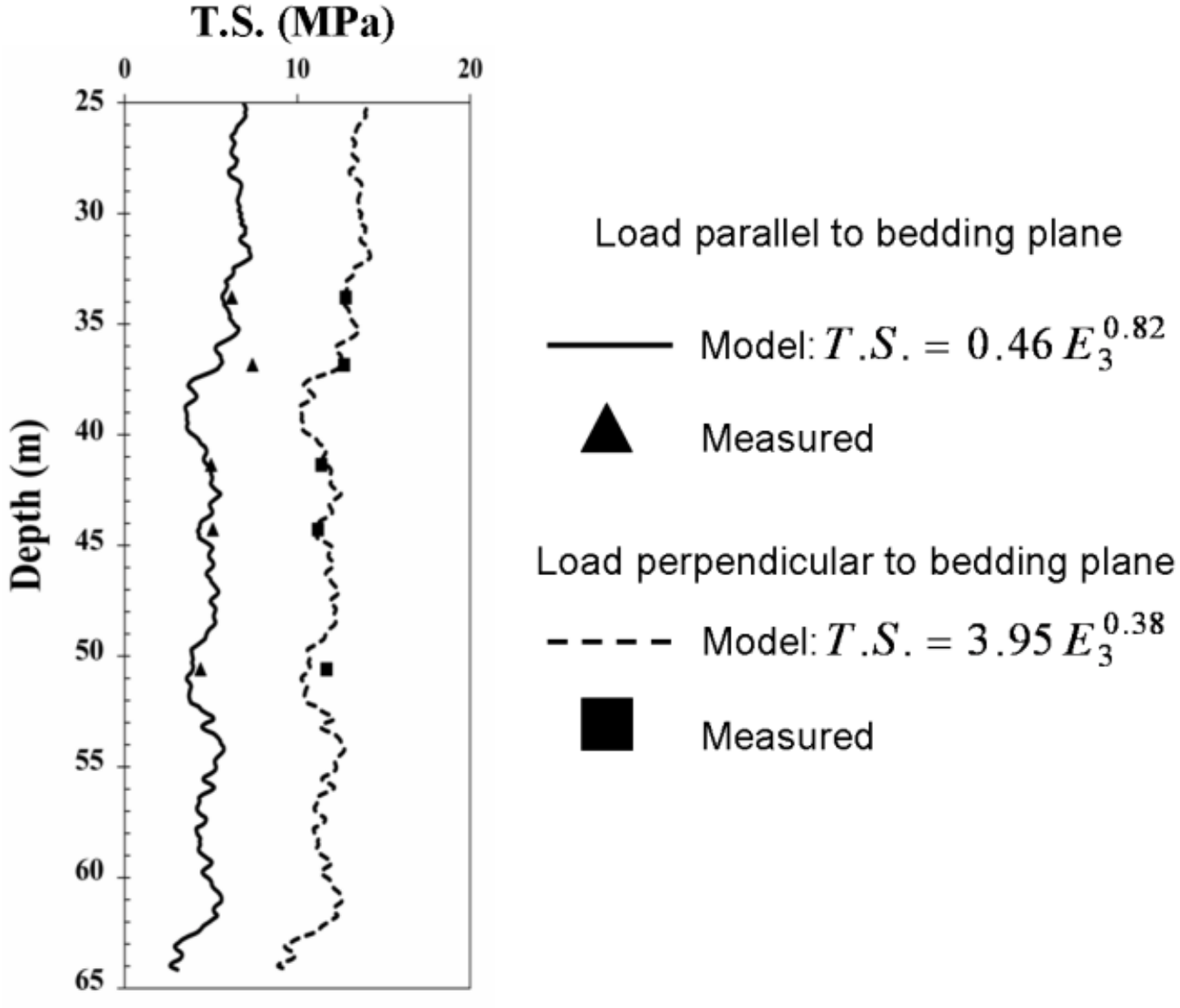

Figure 9. Measured and simulated Woodford shale anisotropic tensile strength.

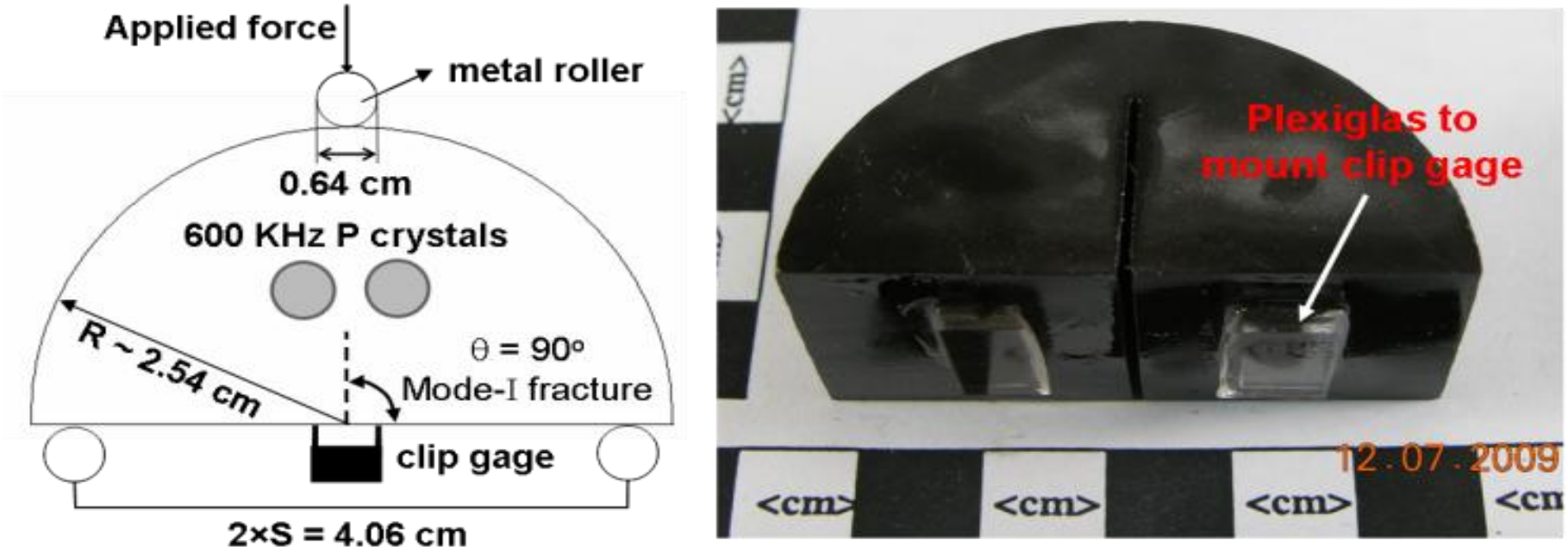

Figure 10. Schematic of the set up and a prepared sample for CNSCB test with acoustic emission recorded.

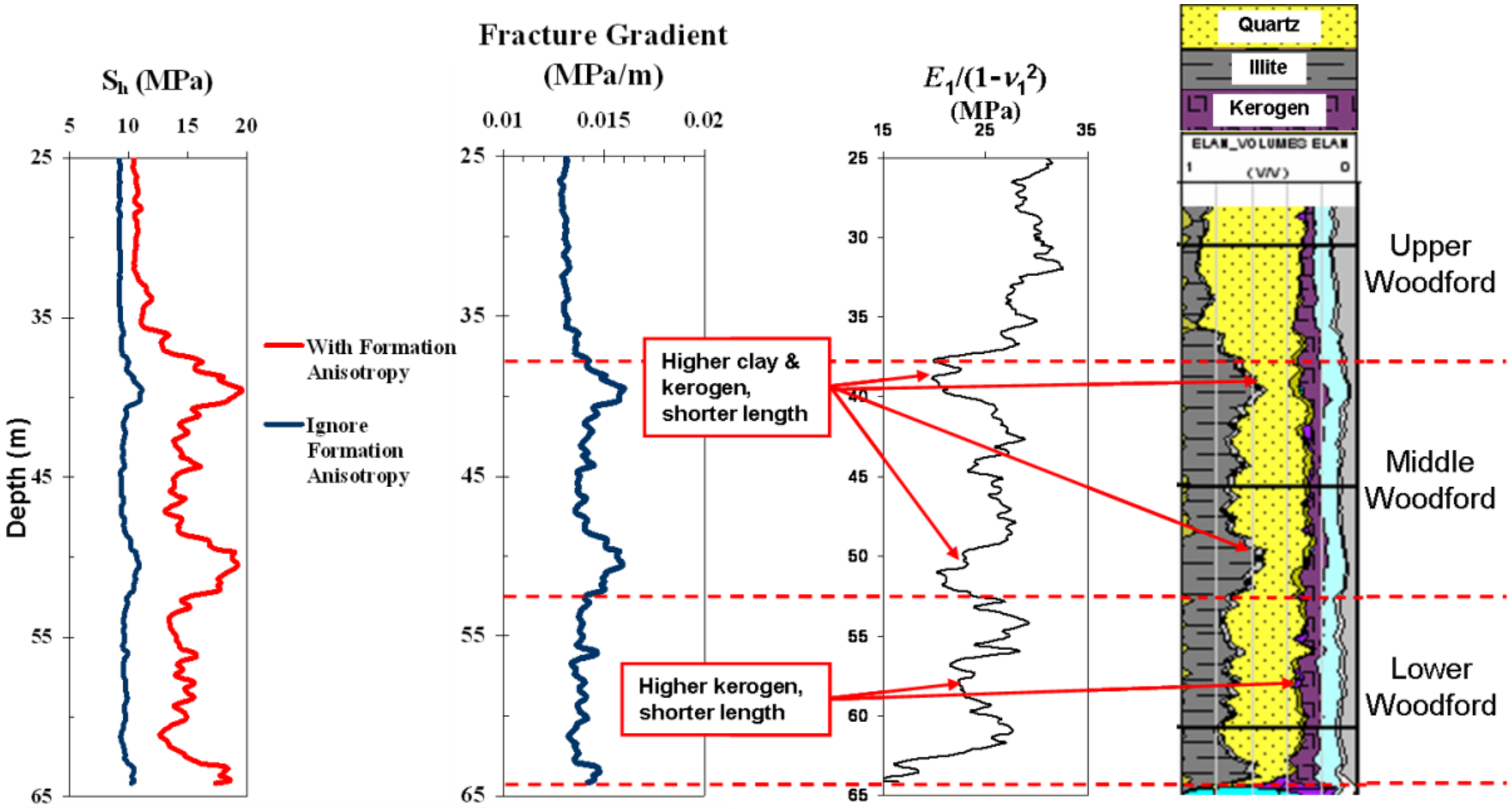

Figure 11. Woodford shale estimated fracture gradient and fracture length profile ($E_1/(1-\nu_1^2)$).

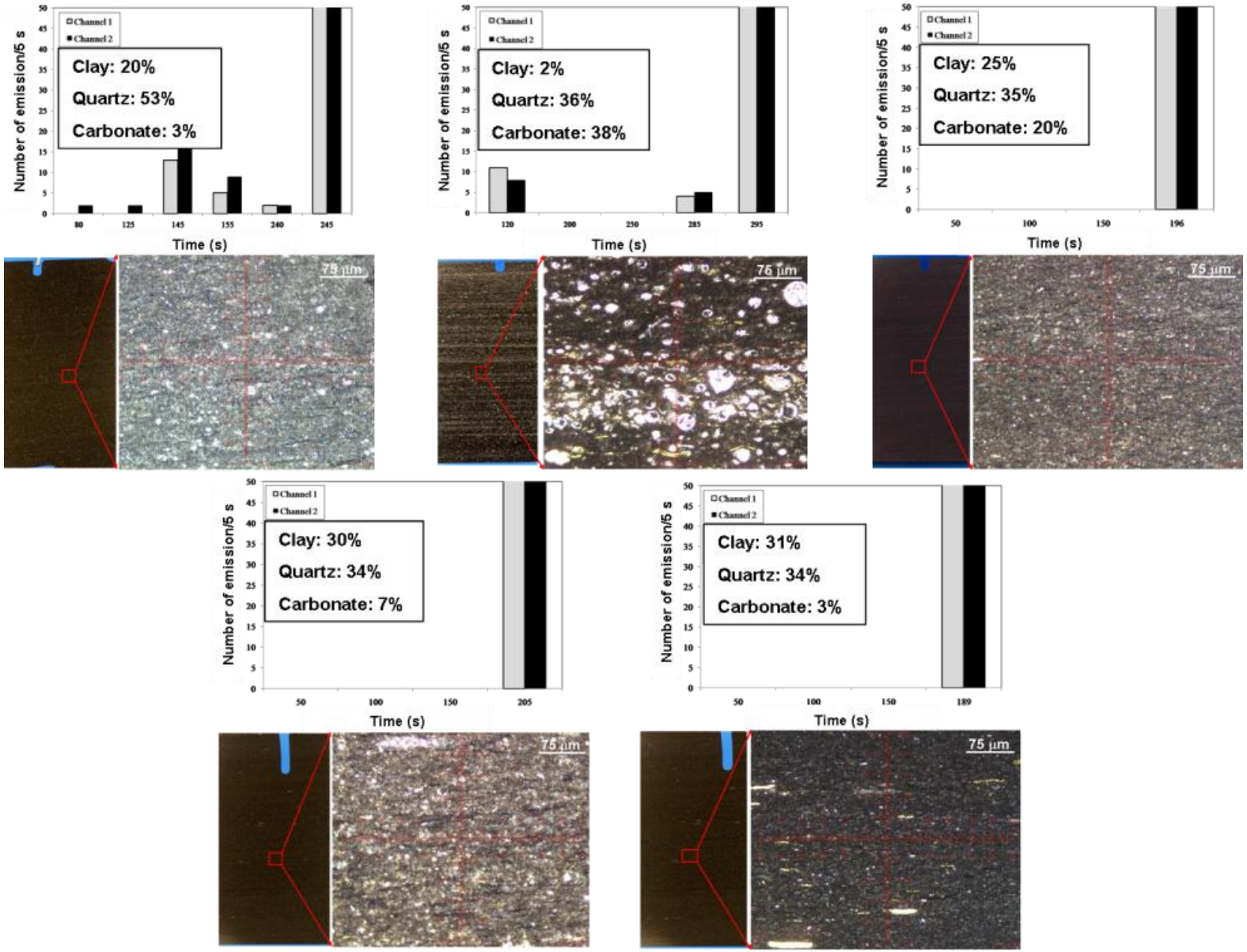

Figure 12. Recorded acoustic emissions during CNSCB test and thin sections of tested samples.

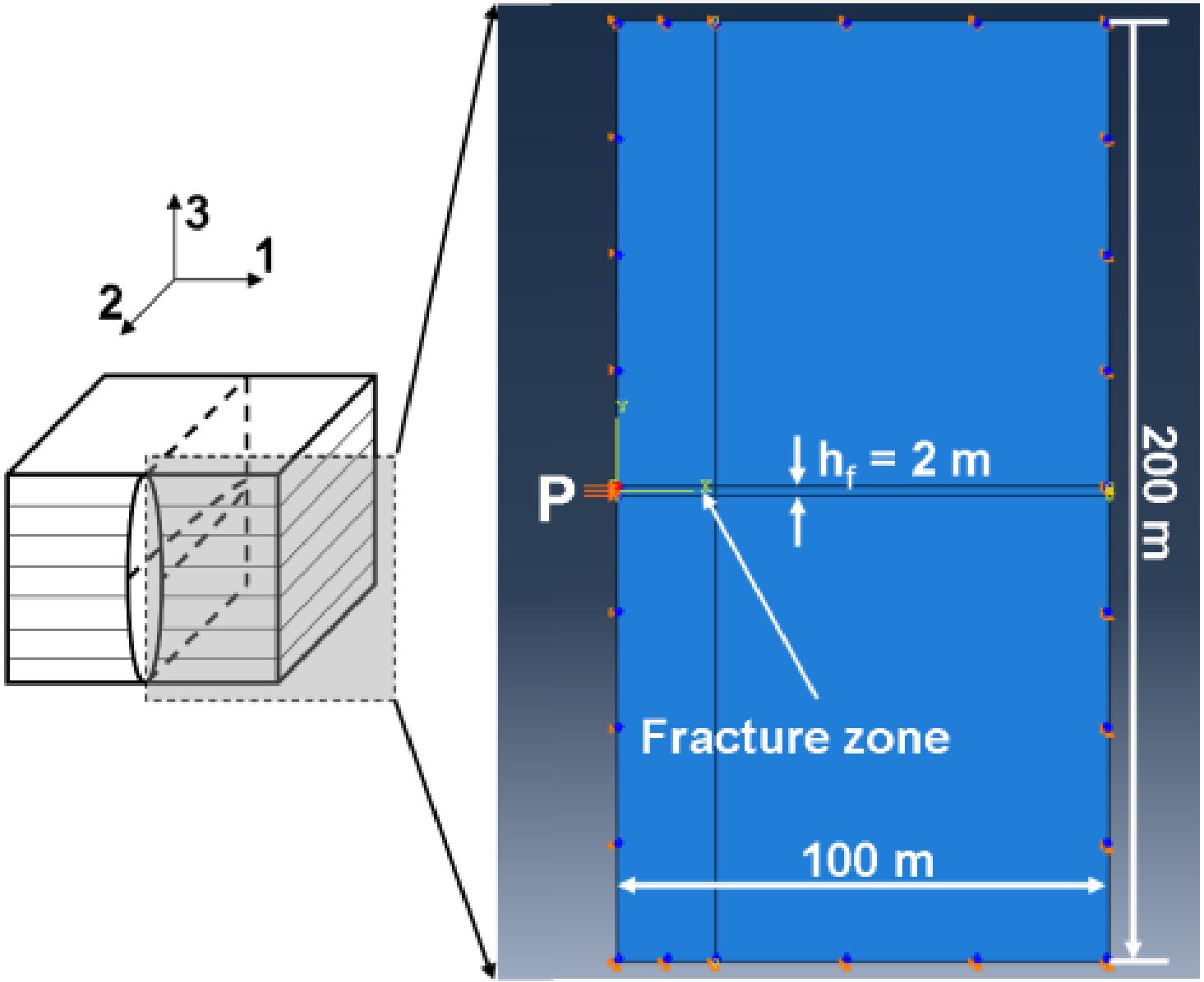

Figure 13. FEM model to investigate shear stress distribution at the vicinity of a hydraulic fracture in transversely isotropic and laminated formation.

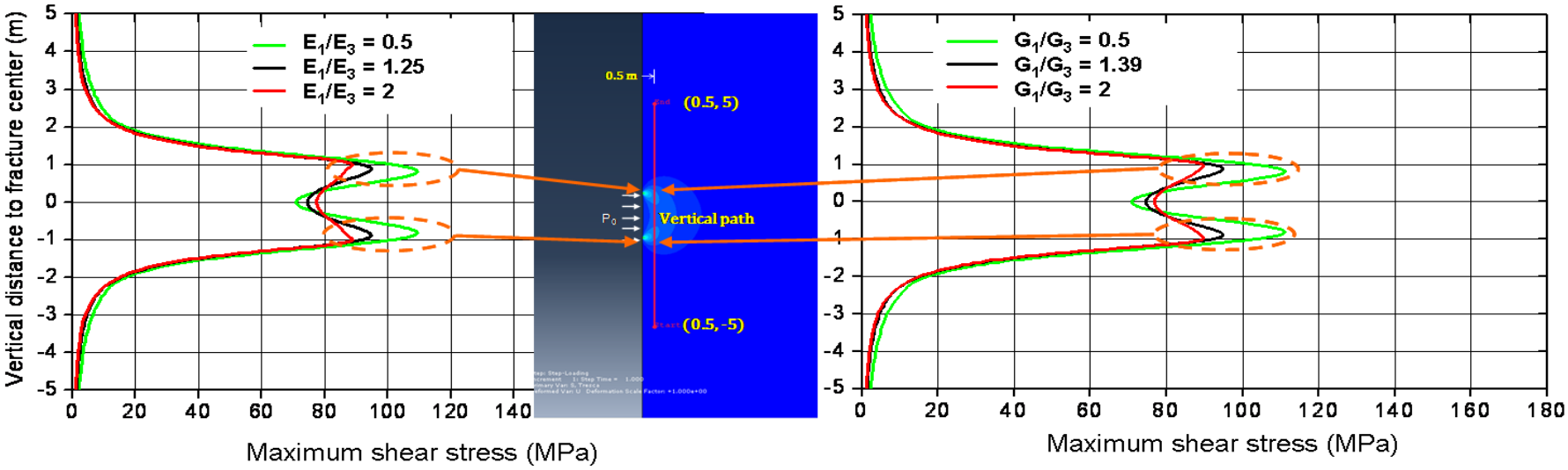

Figure 14. Shear stress distribution along the fracture face at different values of anisotropy ratio.

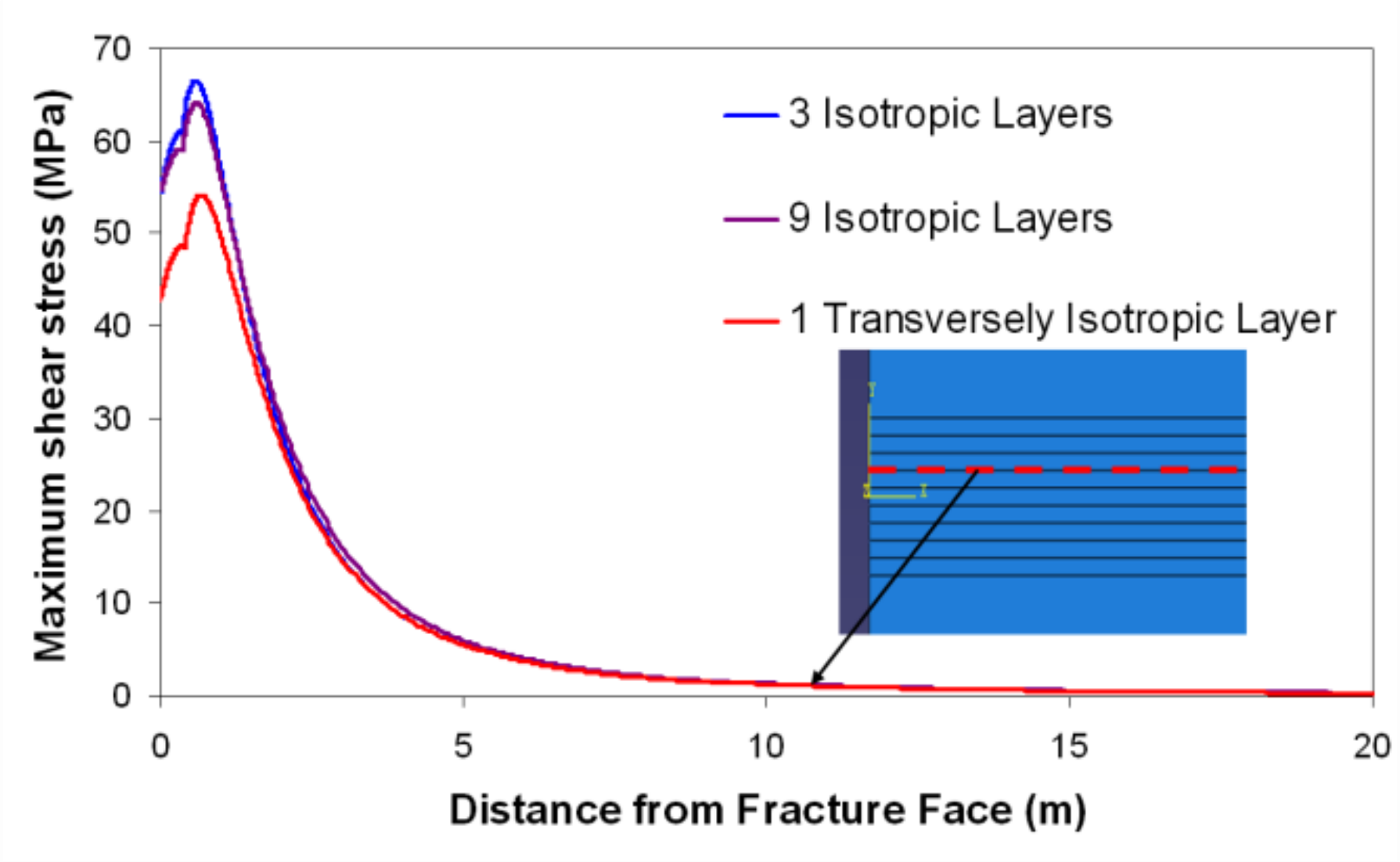

Figure 15. Shear stress distribution along layer interface (same location for all cases).

	Depth (m)	Max. Load (N)	Frac. Toughness (MPa√m)
Upper Woodford	33.81	489	1.17
	36.85	133	1.15
Middle Woodford	41.36	83	0.65
	44.28	89	0.74
Lower Woodford	50.59	89	0.74

Table 1. Summary of CNSCB test results.